Efficient CdSe Nanocrystal Diffraction Gratings Prepared by Microcontact Molding

R. Clayton Shallcross, Gulraj S. Chawla, F. Saneeha Marikkar, Stephanie Tolbert, Jeffrey Pyun, and Neal R. Armstrong*

Department of Chemistry, University of Arizona, Tucson, Arizona 85721

ABSTRACT We describe the formation of efficient transmission diffraction gratings created from patterned high quality ligand-capped CdSe nanocrystals (NCs), using a facile microcontact molding procedure. Soft polymer replicas of commercially available master gratings were "inked" with solvated NCs and the resulting pattern transferred to a variety of substrates after drying. Large-area (>0.5 cm^2), defect free diffraction gratings were prepared with a variety of submicrometer line spacings and feature sizes down to *ca.* 160 nm. The morphology of the resulting pattern was tuned by controlling the concentration of the NC-based ink. Optimized gratings (1200 g/mm) showed an increase in transmission diffraction efficiency (DE) with increasing nanocrystal diameter. DE = *ca.* 15% (488 nm) for 2.5 nm diameter NCs *versus* DE = *ca.* 25−30% (488 nm) for 7.3 nm nanocrystals. These increases in DE are ascribed to changes in both the real (*n*) and imaginary (*k*) components of the complex index of refraction as NC diameter increases. We demonstrate the ability to in- and out-couple incident laser radiation into internal reflection elements using these stamped NC gratings, including single-mode waveguides, offering a novel application of ordered nanocrystal thin films.

KEYWORDS: CdSe nanocrystals · quantum dots (QDs) · microcontact printing · diffraction grating · internal reflection element (IRE) · attenuated total reflectance (ATR) · refractive index

There is significant interest in creating functional nanoparticle assemblies, where metal, metal oxide, and semiconductor nanoparticles are organized *via* strong interparticle interactions (*e.g.*, magnetic nanoparticles),[1−3] printing or molding,[4−7] controlled evaporation techniques,[8] templating/lithographic techniques,[9] or Langmuir−Blodgett techniques.[10−12] Nanoparticles, whose optical properties are modulated by their proximity to one another, may be used as resonators, lasing materials, and related photonic materials.[13−16] Ultrasensitive detection of target analytes may be accomplished with such nanoparticle assemblies by taking advantage of the modulation in the optical properties of the nanoparticles upon adsorption of analytes to the nanoparticle surface.[7] These nanomaterials are usually stabilized by surface capping ligands that vary in structure and chemical composition, which ultimately controls the chemical stability, solubility, and wetting properties as monolayers and multilayer assemblies. We show here the novel use of patterned thin films of ligand-capped CdSe nanoparticles as efficient diffraction gratings. The patterning process is simple and produces gratings with efficiencies rivaling those of ruled gratings in metals or transparent materials.

Efficient diffraction gratings have been formed from nontraditional optical materials such as patterned, electrochemically grown polymers poly(aniline) (PANI) and poly(ethylenedioxythiophene) (PEDOT) on both metal (*e.g.*, Au)[17,18] and metal oxide substrates (*e.g.*, ITO).[19−21] It is understood that the diffraction efficiency (DE) of these materials is strongly dependent on the refractive index contrast between the diffraction material and the superstrate (air, water, *etc.*),[22] and the overall integrity of the diffraction grating features.[18] Many of these patterned polymers are "chemically responsive," in that their diffraction efficiencies change dramatically with changes in chemical composition of the surrounding medium[17,18,21] or of the grating elements themselves.[18,19]

Nanocrystals, especially those created from II−VI semiconductor materials such as CdSe, CdS, and CdTe, *etc.*, show highly tunable optical properties through control of their composition, diameter, shape, and surface-capping ligands.[23] CdSe NCs possess large effective dielectric constants and absorption coefficients that vary with the diameter and composition of the nanocrystal.[24,25] The large effective dielectric and absorptivity, along with the ease of processability, would seem to make ligand-capped CdSe nanocrystals promising candidates as the scattering centers in diffraction gratings operating in the visible and

*Address correspondence to nra@email.arizona.edu.

Received for review July 3, 2009 and accepted September 23, 2009.

Published online October 5, 2009.
10.1021/nn900735y CCC: $40.75

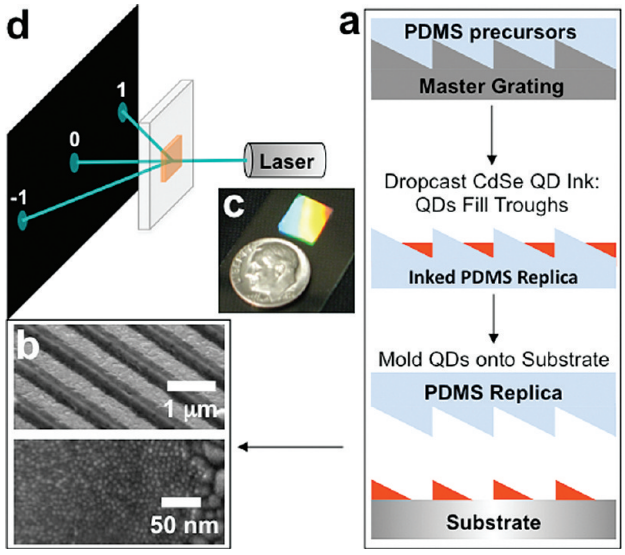

Figure 1. (a) Schematic view of the microcontact molding of ligand-capped CdSe QDs from PDMS replica stamps which affords high-fidelity transfer of master grating features composed of closely packed nanocrystals, over large areas, on transparent substrates; (b) FE-SEM images of transferred QD features as discussed further in Figures 2, 3, and 5; (c) macroscopic view of a high quality microcontact molded grating with a total optically active area of *ca.* 0.6 cm^2; (d) schematic view of the diffraction experiment implemented to determine diffraction efficiency (in either the $m = 1$ or $m = -1$ diffraction spots), as a function of grating fabrication protocols and QD diameter, and ligand coverage.

near-IR wavelength ranges, and as shown here, microcontact molding techniques can be used to routinely create such features.

Microcontact molding/printing techniques utilizing poly(dimethylsiloxane) (PDMS) stamps provide a facile method for patterning of functional materials with high speed and high spatial resolution over large areas.[26] Successful printing of new materials inevitably requires optimization of parameters such as ink concentration, ink−stamp interactions, and ink−substrate interactions. Here we describe the morphology and diffraction efficiency (DE) of diffraction gratings composed of CdSe nanocrystals that are fabricated by microcontact molding using PDMS replicas of aluminum-coated master gratings. Soft grating replicas are "inked" with nanocrystals by drop-casting a defined concentration of CdSe QDs in toluene onto the PDMS stamp and allowing the solution to dry. The CdSe QDs are transferred by bringing the inked PDMS replica into conformal contact with a variety of planar substrates (e.g., glass, tin-doped indium oxide, gold, *etc.*). Large area (>0.5 cm^2) defect-free nanocrystal diffraction gratings with submicrometer features are readily prepared through this molding process with a variety of feature sizes down to *ca.* 160 nm. Optimized nanocrystal gratings (1200 g/mm) show an increase in transmission diffraction efficiency (DE) with increasing nanocrystal diameter, up to *ca.* 30% (using 488 nm laser radiation) for 7.3 nm nanocrystals (the largest diameter investigated in this study). We show that these nanocrystal diffraction grating thin films can act as in- and out-couplers for internal reflection elements (IREs) and single-mode waveguides. To understand the efficacy of using CdSe nanocrystals as the primary component of a diffraction grating, we seek to understand the basic principles of the microcontact molding process and the effect of morphology and nanocrystal size on the measured DE. Subsequent publications will focus on chemical sensor applications of these new grating elements, using both the refractive and luminescent properties of these materials in novel sensor platforms.

RESULTS AND DISCUSSION

Microcontact Molding Process. Figure 1 summarizes the microcontact molding process for these nanocrystal assemblies and shows both optical and field emission scanning electron microscopy (FE-SEM) images of the finished gratings. The molding process began with preparation of a PDMS replica of an aluminum-coated master grating by standard procedures. The "ink" was created from toluene solutions of twice precipitated

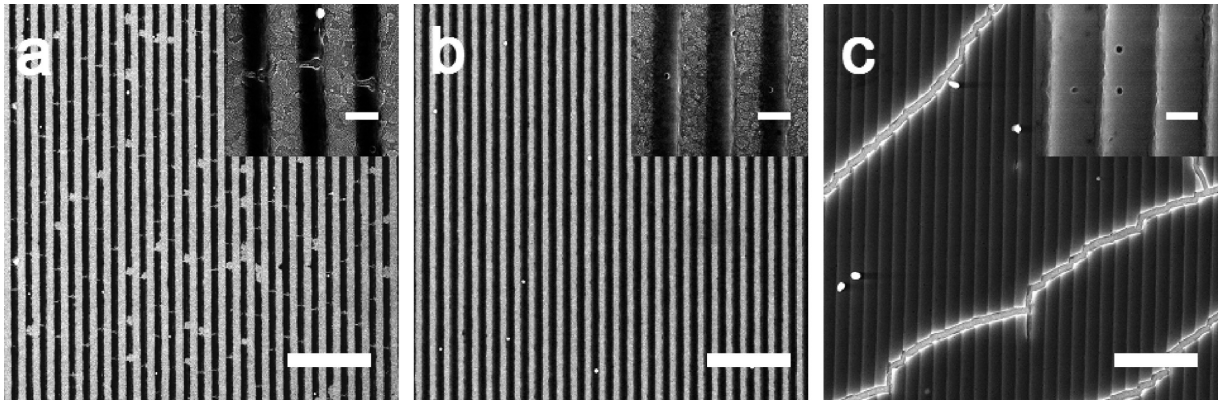

Figure 2. Plane view FE-SEM images of CdSe QD diffraction gratings on ITO-coated glass substrates prepared by microcontact molding from PDMS replicas using different "ink" concentrations (scale bar = 5 μm in main image and 500 nm in inset). (a) Gratings obtained from stamps inked with a low QD concentration (0.1%, w/w), which provides incomplete nanocrystal rows as evidenced by light features (ITO) in otherwise continuous dark rows (QDs); (b) Gratings obtained from stamps with QD ink concentrations in the range 0.5−1.5%, w/w, which provides for coherent nanocrystal features over large areas; (c) increased QD ink concentrations (>2.0%, w/w) transfers a complete nanocrystal layer, which shows cracks and texturing which arise during the drying of the micromolded film.

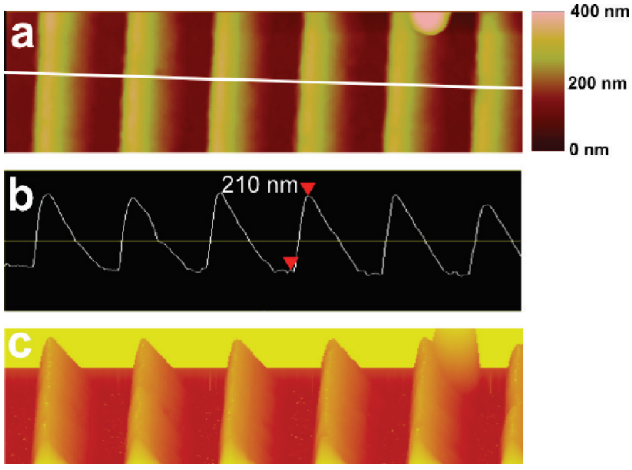

Figure 3. Representative tapping-mode AFM image (5 μm × 1.25 μm) of a CdSe nanocrystal grating on ITO-coated glass prepared from a 1200 g/mm master grating. (a) Plane view showing the cross section line in order to obtain effective grating depth of *ca.* 200 nm. Cross section trace (b) and 3-D image (c) show high fidelity of transfer in that the blaze of the grating is preserved during the microcontact molding process.

(purified) trioctylphospineoxide/hexadecylamine (TOPO/HDA)-capped CdSe nanocrystals.[27] A defined volume (100 μL) and concentration of the nanocrystal "ink" was then dropcast onto a PDMS stamp (1 cm^2), which was held at a low angle (*ca.* 15°) so as to facilitate smooth draining (*i.e.*, no puddling) of the toluene during drying (Figure 1a). Large area defect-free films were created on multiple substrates including gold on glass, glass, and ITO-coated glass. ITO substrates are the focus of this paper because of their transparency for transmission diffraction measurements and conductivity, which is essential for FE-SEM imaging.

FE-SEM images (Figure 1b) of an optimized 1200 g/mm CdSe nanocrystal grating on ITO show highly regular grating features, composed of tightly packed nanocrystals, separated by bare substrate regions void of nanocrystals. The microcontact molding process routinely produced large area (>0.5 cm^2), defect-free nanocrystal gratings (Figure 1c). As-prepared nanocrystal gratings could be mounted normal to incident laser radiation for recording DE data (Figure 1d). It was found that the concentration of nanocrystals used to ink the PDMS stamp had a significant effect on the quality of the transferred nanocrystal gratings, which, in turn, had a considerable effect on the measured diffraction efficiency.

Plane view FE-SEM images in Figure 2 demonstrate the importance of controlling the concentration of the nanocrystal solution used to ink the PDMS stamp in order to influence the morphology of the transferred grating features. In this study, a total of five concentrations (0.1, 0.5, 1.0, 1.5, and 2.0%, w/w in toluene) were used to ink the PDMS stamps; however, only three images are shown in detail, representing the full range of morphologies that could be achieved. Inking the stamp with relatively low concentrations of nanocrystals (0.1 wt %) produced somewhat irregular grating features as evidenced by bright (ITO) regions separating the otherwise continuous dark rows of nanocrystals (Figure 2a). Figure 2b is representative of gratings obtained from PDMS stamps inked with CdSe NC solutions with concentrations in the range of 0.5−1.5 wt %. A representative tapping-mode atomic force microscope (AFM) image (Figure 3) of our best 1200 g/mm gratings demonstrates that the molding process affords transfer of high fidelity features, which maintain a blaze angle in each feature similar to the master grating with nanocrystal features that range in height from 180 to 220 nm, with an average of *ca.* 200 nm. If the concentration of the nanocrystal inking solution was increased to 2.0% or greater, large areas of the PDMS stamp were totally covered with a film of nanocrystals, which transferred as a continuous textured film without any visible substrate between nanocrystal grating features (Figure 2c). These thick nanocrystal films were almost always cracked, most likely originating from the original drying process on the PDMS stamp. Our diffraction data (*vide infra*) suggests that complete nanocrystal features separated by substrate regions devoid of any nanocrystals (Figures 1b and 2b) is the optimum morphology for a nanocrystal diffraction grating.

The full range of concentrations studied here suggested that there was a critical solution concentration of ligand-capped NCs that must be met in order for continuous features to be created in the troughs of the PDMS stamp. Previously, it has been demonstrated by Bawendi and co-workers that chemical compatibility of both the solvent and ligand-capped NC with the templating substrate (*i.e.*, PDMS) has a significant influence on the morphology of quantum dot films.[4] For the low to midrange ink concentrations (*i.e.*, ≤ 1.5 wt %) used in this study, the transferred QD grating features were separated by bare substrate regions, which indicated that the nanocrystal ink must be sequestered in the troughs of the PDMS stamp during drying by an intertrough dewetting process (Figure 4a). Increased NC concentrations (≥2.0 wt %) provided continuous textured NC films, which implied that dewetting does not occur at these elevated concentrations. These observations suggested that weak nanocrystal−nanocrystal or nanocrystal−PDMS interactions played a critical role in the self-organization of the CdSe NCs on the PDMS substrate.

For low and midrange NC concentrations, the incompatibility of toluene-based ink with the PDMS substrate dominated the initial intertrough dewetting process, which led to droplets of ink forming in individual troughs (Figure 4a). Furthermore, the lateral continuity of the transferred NC features was dependent on the CdSe NC concentration (Figure 4b), which indicated

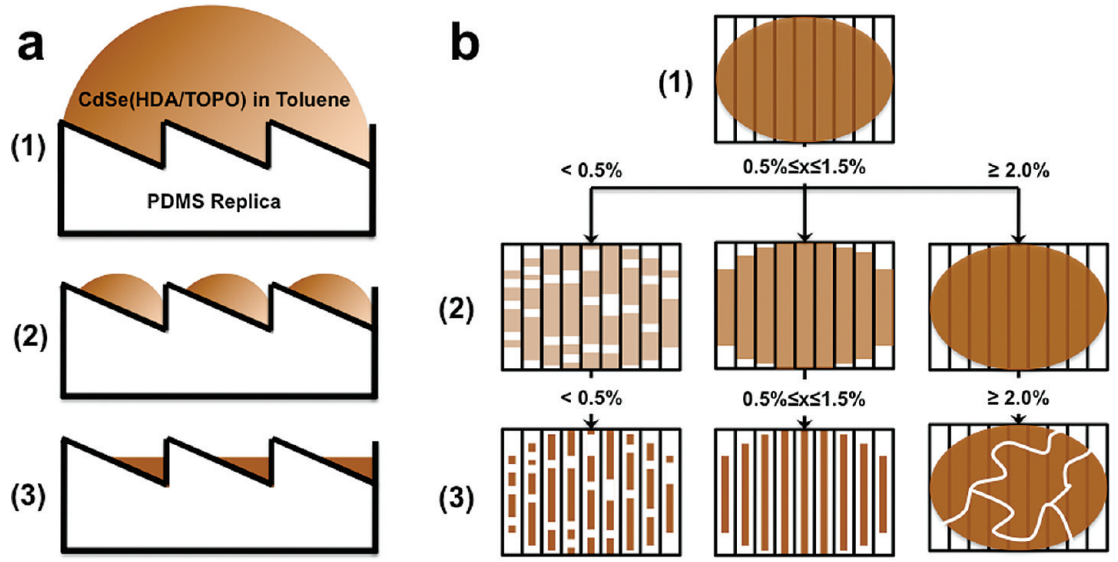

Figure 4. Schematic illustration of the concentration-dependence of CdSe QD ink wetting/dewetting and drying processes on PDMS replica stamps. (a) Cross-section view of (1) CdSe NC ink just after dropcasting on a PDMS stamp for all ink concentrations; (2) intertrough dewetting of the ink during drying provides for individual droplets to form in each trough for moderate ink concentrations (≤1.5 wt %); (3) these individual droplets fully dry to provide CdSe NC solids in the troughs of the stamp. (b) Top view of dewetting and drying process for all ink concentrations: (1) after the ink is dropcast, (2) intertrough dewetting of the ink occurs on the PDMS stamp for low to midrange concentrations (≤1.5 wt %), while dewetting is not observed for higher ink concentrations (≥2.0 wt %). Further intratrough dewetting (droplet rupture) was observed for low concentrations (≤0.5 wt. %). (3) These wetting/dewetting processes provided for incomplete NC grating features for low concentrations, while highly regular features are observed for the midrange concentrations. Finally, the lack of dewetting for high NC concentrations afforded thick CdSe NC films that showed cracking due to capillary forces that dominated as the films dried.

that the ligand-capped NCs played a critical role in the intratrough drying/dewetting process in the individual PDMS channels. van der Waals interactions between the solvated NCs (NC−NC interactions) and/or the NCs and the PDMS (NC−PDMS interactions) in the middle concentration range (*i.e.*, 0.5−1.5 wt %) prevented rupturing of individual trough droplets, which allowed further drying to produce continuous nanocrystal features over extensive length scales. Discontinuous features for low solution concentrations (0.1 wt %) resulted from rupturing of individual trough droplets due to an intratrough dewetting process arising from more dominant toluene−PDMS interactions. Dewetting was not observed for high NC concentrations (≥2.0 wt %), as evidenced by continuous NC features that were not separated by bare substrate, which indicated that at such high concentrations, nanocrystal−nanocrystal and/or nanocrystal−PDMS interactions dominated in the final drying process. Significant capillary forces produced strain in these thick films during drying, which caused cracking of the final film.

To determine the minimum feature size obtainable for these nanocrystal assemblies, four aluminum-coated master gratings (1200, 1800, 2400, and 3600 g/mm) were investigated. The 1200 g/mm master is blazed (blaze angle = 36°), while the remaining higher groove density masters are holographic. Figure 5 shows FE-SEM images of the nanocrystal gratings stamped from the aforementioned four master grating molds (all were inked with 0.5% nanocrystal solutions) on ITO substrates. Each mold transfers high quality periodic nanocrystal rows (darker visibly raised areas) separated by regions of bare ITO substrate (textured bright areas representative of the subgrain structure of these sputter-deposited ITO films).[28] High resolution FE-SEM images were able to resolve individual stamped nanoparticles with core diameters down to *ca.* 2.5 nm.

The 1200 g/mm nanocrystal gratings maintained a blaze similar to the master, while the remaining three higher density nanocrystal gratings have features with a more Gaussian shape, similar to the holographic masters. Using plane view SEM images (Figure S1), we were able to measure the transferred nanocrystal feature width (*w*) and the grating spacing (*d*), which are summarized in Table 1. All four nanocrystal gratings are efficiently transferred with close agreement between the theoretical gratings spacing and the measured value of the QD features. A minimum feature width of 160 ± 10 nm was obtained for both the 2400 and 3600 g/mm samples, corresponding to an average range of *ca.* 17−36 close-packed nanocrystals along the base of each feature for the largest (7.3 nm) to smallest (2.5 nm) nanocrystal diameters explored (assuming a ligand length of *ca.* 1 nm). Feature heights of *ca.* 100 nm consisted of *ca.* 11−22 close-packed nanocrystals for the range of 7.3−2.5 nm diameter cores. We see no reason that smaller feature sizes (down to a few nanoparticles in height and width) could not be realized with even higher resolution masters.

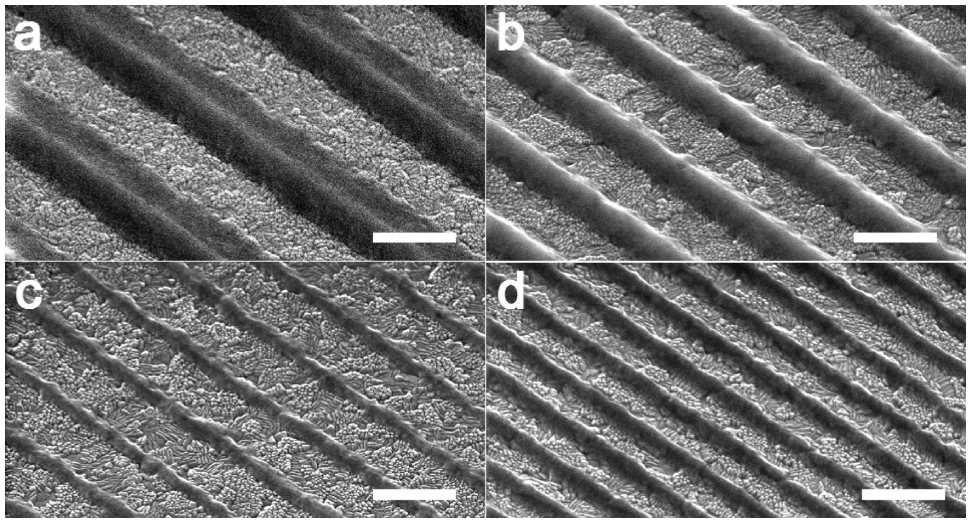

Figure 5. Perspective (45°) FE-SEM of CdSe QD gratings prepared by microcontact molding from PDMS replicas made from increasing groove density master gratings (scale bar = 500 nm in each image). Image a was taken from a film prepared using a blazed master with 1200 grooves/mm while the films in images b, c, and d were prepared from holographic masters with 1800, 2400, and 3600 grooves/mm, respectively.

Evaluation of the DE of 1200 g/mm QD Gratings on ITO. DE was measured for nanocrystal gratings in a transmission geometry at normal incidence with nonpolarized argon-ion (488 nm) and HeNe (633 nm) laser excitation. The microcontact molding process produces regularly spaced semiconductor nanocrystal features that afford a periodic modulation of the wavelength-dependent complex index of refraction [$n'(\lambda) = n(\lambda) + ik(\lambda)$], which is the basis for diffraction of incident radiation (n and k are the refractive index and absorptivity, respectively).[22] Constructive interference of an incident beam, normal to the grating, produces a diffraction pattern and is described by the grating formula

$$m\lambda = d \sin\theta \quad (1)$$

where m is the diffraction order, λ is the wavelength of the incident radiation, d is the spacing of the periodic features, and θ is the angle at which diffraction occurs (Bragg angle). The measured DE of any grating material may be defined as:

$$\mathrm{DE} = \frac{\Sigma I_{\mathrm{diff}}}{I_{\mathrm{o}}} \quad (2)$$

where I_{diff} is the intensity of the diffracted beam and I_{o} is the intensity of the incident beam. While the DE is dependent on the difference between both the real (n) and imaginary (k) components of the complex refractive index with the surrounding medium (air in this case) separating the grating features, it is also a function of the grating thickness (T) and the optical density (OD) of the sample.

$$\mathrm{DE} = \left(\exp\left(\frac{-2.303\mathrm{OD}(\lambda)}{\cos\theta}\right)\right)\left(\frac{\pi T}{\lambda\cos\theta}\right)^2[\Delta k(\lambda)^2 + \Delta n(\lambda)^2] \quad (3)$$

Schanze *et al*. demonstrated that small changes in n and k do in fact give detectable changes in DE.[19] In our earlier work with diffraction gratings created from conductive polymers,[28] and in the studies of conducting polymer gratings from Hupp and coworkers,[21] it was confirmed that changes in the real component of refractive index (n) are more significant than changes in k.

An optimization curve showing the relationship between DE (488 and 633 nm) and ink concentration for a representative sample size of nanocrystals (4.1 nm) is plotted in Figure 6a. There was an initial increase in DE with increasing the QD ink concentration from 0.1 to 0.5% (w/w), then a region where DE was nearly constant (up to 1.5 wt %). Once the concentration was finally increased to 2.0% (w/w), the DE almost always decreased. This trend can be understood by closely examining the morphology of the nanocrystal gratings as a function of inking concentration (*vide supra*) and its relationship to eq 3. All nanocrystals stamped with a 0.1 wt % ink concentration produced discontinuous grating features as depicted in Figure 2a. These defective grating features likely scatter the incident radiation at angles and planes not aligned with coherent processes producing the dominant diffraction pattern in the detection plane, thus lowering the DE. Furthermore, these incomplete grating rows provided decreased DEs due to a lower effective refractive index, since air occupied significant portions of the grating. The increased DE for intermediate concentrations was di-

TABLE 1. Diffraction Grating Parameters for the Master Gratings *versus* CdSe QD Diffraction Gratings

master (g/mm)	d (master) (nm)	d (QD grating) (nm)	w (QD grating) (nm)
1200	833	840 ± 30	510 ± 20
1800	556	540 ± 30	310 ± 10
2400	417	420 ± 30	160 ± 10
3600	278	270 ± 40	160 ± 10

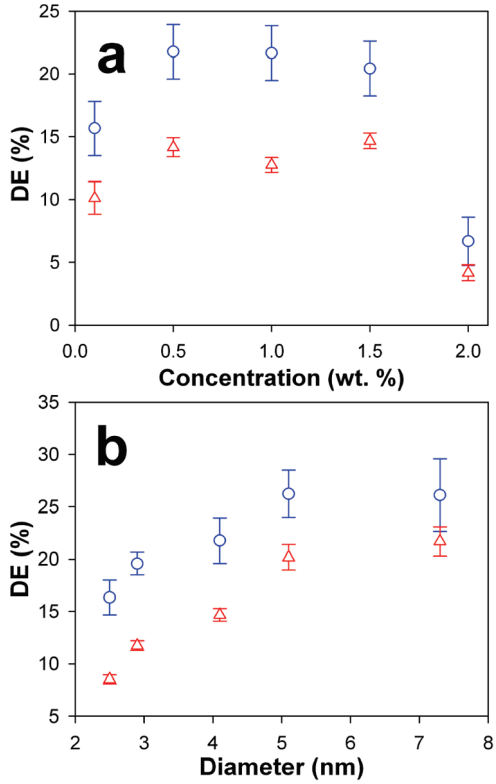

Figure 6. Diffraction efficiency measurements as a function of (a) QD ink concentration and (b) nanocrystal diameter for 488 nm (blue circles) and 633 nm (red triangles) laser excitation. The data in panel a is representative for all nanocrystal sizes used in this study and relates to the middle diameter of 4.1 nm. The remaining curves for all sizes can be found in Supporting Information Figure S2.

rectly related to a convergence of individual grating features, producing a continuous periodic modulation of the complex refractive index (Figure 2b). Further increasing the inking solution concentration to 2.0 wt % decreased the measured DE due to a combination of increased OD for thick nanocrystals films, which should exponentially lower DE according to eq 3, and incoherent scattering produced by the cracked regions.

The DE measured at 488 and 633 nm for the five nanocrystal sizes used in this study, ranging from 2.5 to 7.3 nm in diameter, increased with increasing nanocrystal diameter (Figure 6b). The increase in DE is due to both a change in absorptivity (k) and refractive index (n) as a function of nanocrystal diameter. It is well-known that the optical band gap decreases, while the oscillator strength increases, as the diameter of quantum confined (up to *ca.* 10 nm) CdSe nanocrystals increases.[25] All the nanocrystals used in this study efficiently absorb 488 nm radiation ($>10^4$ L mol^{-1} cm^{-1}), while the absorptivity at 633 nm is lower in all cases (Table 2 and Figure S3). Therefore, the discrepancy in DE between 488 and 633 nm for each size of nanocrystal may be rationalized by a significant difference in molar absorptivity (k). Since there is not an appreciable absorption at 633 nm for the smallest NC sizes (*i.e.*, 2.5 and 2.9 nm), the measured difference in DE must be due primarily to differences in the effective refractive index.

TABLE 2. Summary of the Maximum Diffraction Efficiency (DE) As It Relates to the Solution Molar Absorptivity (ε) and Percent Ligand Mass of CdSe QDs

diameter[a] (nm)	max DE (488 nm, %)	max DE (633 nm, %)	ε[a] (488 nm, L/mol · cm)	ε[a] (633 nm, L/mol · cm)	ligand mass %[b]
2.5	16 ± 2	9 ± 1	2.52 × 10(4)	5.25 × 10(1)	30
2.9	20 ± 1	12 ± 1	4.55 × 10(4)	4.54 × 10(2)	27
4.1	22 ± 2	15 ± 1	3.55 × 10(5)	6.20 × 10(3)	20
5.1	26 ± 2	20 ± 1	7.71 × 10(5)	8.35 × 10(4)	17
7.3	26 ± 3	22 ± 1	3.85 × 10(6)	1.07 × 10(6)	10

[a]Diameter and molar absorptivity (ε) at the first exciton peak was calculated from the spectra in Figure S3 using formulas provided in ref 25. A two point calibration using the calculated value for the first exciton peak and zero for a far red wavelength (850 nm) was then used to estimate an extinction spectra for each sample, thus providing an estimate for the molar absorptivity at 488 and 633 nm. [b]Percent ligand mass was measured by performing TGA on purified samples (Figure S4).

We assume that the effective refractive index of any solid composed entirely of nanocrystals is dependent *in part* on the ratio of the refractive indices of the low dielectric organic ligands and nanocrystal core, with a significantly higher dielectric constant. Thermogravitational analysis (TGA), which quantitates mass loading of ligands in the quantum dot solid, should be directly related to the effective refractive index of the nanocrystal film. This hypothesis also assumes that the mass loss in the TGA experiment was solely due to removal of ligands from the dried nanocrystal solid, while the remaining mass is representative of the core alone.[29] This assumption does not take into account any void spaces in the film that may be taken up by air, which would also lower the observed refractive index.[30] Our TGA data (Figure S4), which is summarized in Table 2, for a series of purified (2× precipitated) CdSe nanocrystals shows a decrease in the relative ligand mass with increasing diameter, as predicted by Foos and coworkers.[29] We infer that the decrease in ligand mass with increasing diameter is correlated to an increase in the effective refractive index (n) of the nanocrystal feature in each grating, which, along with an increase in absorptivity, provides for increased DE for both 488 and 633 nm laser excitation.

To elucidate the effect of ligand mass on DE, a precipitation study was performed in which DE was measured for gratings molded with nanocrystal ink (created from *ca.* 4 nm diameter CdSe QDs) that was subjected to a varying number of precipitation/purification steps (Figure 7a). TGA data shows a decrease in the effective ligand mass (determined from the overall mass loss in the TGA experiment) with increasing precipitation (purification), which removes excess ligand not permanently bound to the QD surface (Figure 7b). We observed a significant increase in DE after one precipitation, which was due to our inability to make high quality gratings with the as-prepared (unpurified) nanocrys-

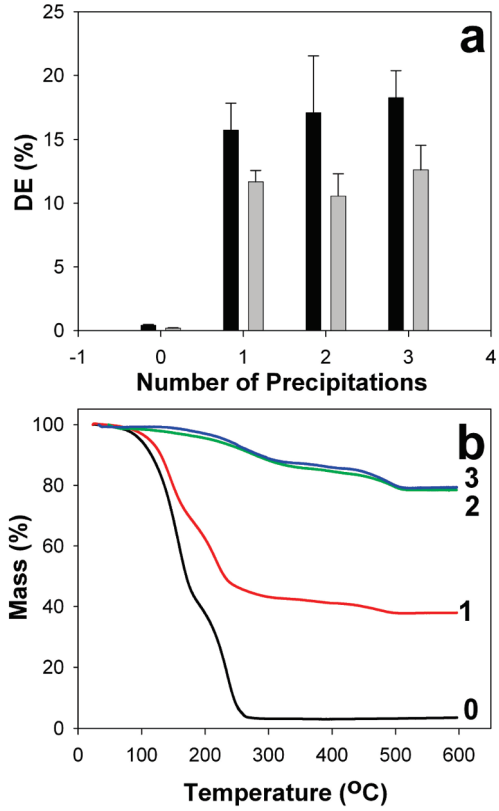

Figure 7. (a) Diffraction efficiency as a function of number of precipitations during removal of excess ligand during QD purification for both 488 nm (black) and 633 nm (gray) laser excitation; (b) mass percent (determined from TGA) for a single batch (~4 nm) of CdSe QDs with increasing number of precipitations during cleanup, ranging from zero precipitations to 1, 2, and 3 precipitations.

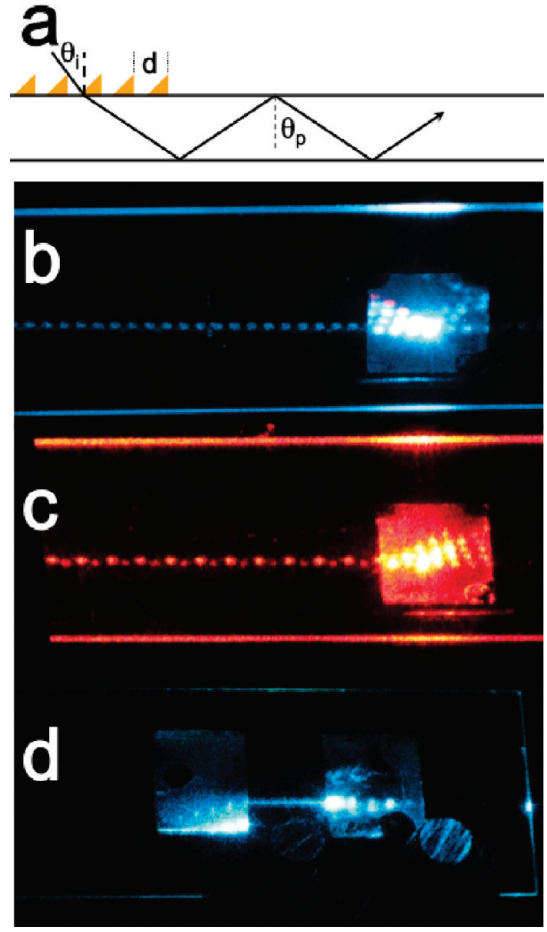

Figure 8. (a) Schematic view of the use of a QD grating for in-coupling of either 488 or 632 nm light into an internal reflection element (IRE), at an incident angle of θ_i with propagation angle θ_p, using a grating with spacing *d*. Both 488 (b) and 633 nm (c) radiation can be coupled into a 0.5 mm thickness glass slide using QD gratings (right-hand side of each figure), as evidenced by the internally reflected laser spots in the IRE when viewed from above; (d) QD gratings can also be used to both in-couple (right) and out-couple (left) the 488 nm laser line into a single-mode planar sol−gel waveguide (*ca.* 300 nm thickness).[32]

tal solids that are composed of greater than 95% ligand. There was a general increase in DE for gratings prepared with solutions precipitated from a total of one to three times, which corresponds to a decrease in effective ligand mass in the nanocrystal solid. We interpret this observed increase in DE for both 488 and 633 nm as an increase in the relative refractive index of the nanocrystal solids due to the removal of excess ligand. It is important to note that the locations used to measure DE for the gratings molded using inks precipitated either one, two, or three times all had comparable ODs and grating thickness, which has a substantial effect on the measured DE, as shown in eq 3.

CdSe QD Coupling Gratings. The nanocrystal gratings presented here are ideal candidates for constructing optical coupling elements owing to their ease of fabrication and the ability to control feature size by choice of master template and size of the nanocrystal. Figure 8a is a simplified diagram whereby incident radiation is coupled into and subsequently trapped inside an internal reflection element (IRE).[31] The light must be coupled into the substrate at an angle that satisfies Snell's law for total internal reflection (i.e., light incident at the IRE/superstrate interface is reflected rather than refracted). Figure 8 panels b and c show photographs of an 1800 g/mm nanocrystal diffraction grating coupling both 488 and 633 nm laser radiation into an ITO-coated glass slide, confirmed by the internally reflected laser spots at the slide/air interface. To further demonstrate the utility of our CdSe QD gratings, we were able to couple radiation into a TiO_2/SiO_2 single mode sol−gel waveguide,[32] (an extremely thin IRE on the order of 300 nm in thickness) utilizing an 1800 g/mm element. The in-coupled radiation was no longer visible as internally reflected spots, but rather as a streak of light that was out-coupled by another nanocrystal grating. These images are only a first step to demonstrate that CdSe nanocrystal gratings can in fact diffract light at angles necessary to satisfy conditions for internal reflection in both single mode and multimode waveguide IREs. Further studies will further quantify the coupling parameters and utilize these elements as attenuated total reflectance spectroscopic platforms.

CONCLUSION

Microcontact molding of CdSe nanocrystals offers a facile route for preparation of efficient diffraction gratings on various substrates. The concentration of purified nanocrystal solutions used to ink the PDMS stamp had a significant effect on both the morphology and DE of blazed 1200 g/mm gratings, which was optimized in the region of 0.5−1.5 wt %. We determined that concentration-dependent wetting/dewetting processes during the ink-drying step on the PDMS stamp were responsible for the transferred nanocrystal grating morphologies. Submicrometer nanocrystal grating features could be transferred down to a line spacing (*d*) of *ca.* 270 nm (160 nm in width and 100 nm in height). Optimized QD gratings were continuous, extremely regular, and produced defect free films with areas greater than 0.5 cm^2. The DE of 1200 g/mm gratings produced with CdSe nanocrystals ranging from 2.5 to 7.3 nm in diameter increased with increasing diameter (up to *ca.* 30% for 488 nm radiation). The increase in DE for both excitation wavelengths studied as a function of nanocrystal diameter was attributed to both an increase in molar absorptivity and refractive index with increasing diameter. While the molar absorptivity of the nanocrystals is well-known as a function of size, the real component of the refractive index is less understood. We utilized a simple argument for the relative refractive index of nanocrystal solids that used TGA data to determine the ratio of nanocrystal core mass to that of the ligands (*i.e.*, a decreased ligand mass should account for a larger effective refractive index). It was shown that purified nanocrystal solids without excess ligand provided the highest DEs, confirming our hypothesis. The as prepared nanocrystal gratings showed promise as optical coupling elements for both thick internal reflection elements and extremely thin sol−gel waveguides, which offers novel application diffraction gratings composed of ligand-capped nanocrystals.

METHODS

Materials. Cadmium oxide (~1 μm, 99.5%), selenium powder (~100 mesh, 99.5%), technical grade (90%) trioctylphosphineoxide (TOPO), tributylphosphine (TBP, 97%), stearic acid (SA, 99%), and hexadecylamine (HDA, 90%) were purchased from Aldrich. Chloroform (EMD, ACS grade), toluene (EMD, OmniSolv) and acetone (EMD, ACS grade) were purchased from VWR. Ethanol (absolute) was purchased from Decon Laboratories, Inc. The PDMS precursors (SYLGARD silicone elastomer 184 and SYLGARD 184 curing agent) were obtained from Dow Corning. Triton-X was purchased from Alfa Aesar. Glass slides, ITO-coated glass (15 Ω/cm^2), and Au-coated glass (glass/5 nm Ti/100 nm Au) were purchased from VWR, Colorado Concept Coatings, LLC, and Evaporated Metal Films, respectively.

CdSe Nanocrystal Synthesis.[27] Standard Schlenk procedures were used during the synthesis process. In a typical synthesis, a selenium injection solution was prepared in a glovebox under nitrogen. The solution was prepared by mixing selenium (0.510 g, 6.46 mmol) and TBP (6.25 mL) in a scintillation vial. After ~30 min, the suspended selenium became soluble to afford a light yellow solution. The vial was capped with a rubber septum prior to removal from the glovebox. CdO (0.0983 g, 0.766 mmol) and SA (0.8974 g, 3.15 mmol) were loaded into a 50 mL 3-neck round-bottom flask with a PTFE stir bar. The flask was fitted with a thermocouple and heated to 150 °C in air. After ~30 min, the reddish-brown slurry became optically clear indicating formation of cadmium stearate. To the hot reaction vessel, HDA (9.73 g, 40.3 mmol) and TOPO (9.83 g, 25.4 mmol) were added through a glass funnel. The flask was fit with a condenser and heated to 120 °C with stirring under vacuum for 30 min to remove excess O_2. The reaction flask was backfilled with Ar and heated to 320 °C. At this temperature, the selenium solution was swiftly injected into the reaction flask. Upon injection, the solution temperature dropped to 280 °C. The solution was maintained at 280 °C for 3 min and was then removed from the heating mantle and allowed to cool to ~70 °C, where $CHCl_3$ (50 mL) was added. The solution was then placed in a refrigerator overnight and all following procedures were performed in air. A whitish/red solid formed on the top of the nanoparticle solution and was discarded. The nanoparticles were precipitated (purified) two times with acetone from $CHCl_3$ solution to remove excess ligand. The final precipitate (ranging from 50 to 200 mg of purified particles) was dissolved in hexanes and centrifuged at 8000 rpm for 20 min and filtered through a 0.2 μm PTFE filter and dried down with Ar to get the final mass of particles, which were then dissolved in a defined mass of toluene to provide the ink solution. It should be noted that in order to obtain smaller particles the injection temperature was as low as 230 °C; however, larger particles were obtained by increasing the injection temperature up to 350 °C. Furthermore, reaction time was varied to provide further size control (*i.e.*, shorter reaction times provide for smaller nanocrystals; however, nanocrystals may become polydisperse at excessive reaction times).

Microcontact Molding Process. PDMS replicas were produced using one blazed (1200 grooves/mm, blaze angle = 36°) and three holographic (1800 g/mm, visible; 2400 g/mm, UV; 3600 g/mm, UV) aluminum-coated master gratings. A PTFE container which held the masters was filled with a well-mixed (~1 min) gel of 10:1 (w/w) of SYLGARD silicone elastomer 184 and SYLGARD 184 curing agent covered and allowed to rest for *ca.* 1 h in order to completely degas, freeing all air bubbles. An oven (120 °C, 1.5 h) was used to speed up the PDMS curing process. Prior to inking the PDMS replicas, the desired concentration of NPs were filtered through a 0.2 μm PTFE disk filter and then sonicated for 15 min. The stamp was then "inked" by dropcasting 100 μL of a well-dispersed nanocrystal solution in toluene onto an angled (*ca.* 15°) PDMS substrate (sonicated for 15 min in ethanol after removal from the mold) and allowed to dry in a covered Petri dish. Glass and ITO-coated glass were cleaned by successively sonicating in aqueous Triton-X solution (10%, v/v), nanopure water (18 MΩ cm), and finally ethanol. These substrates were then dried under a stream of N_2 and O_2 plasma-etched (15 mW, 15 min). Au-coated glass substrates were cleaned by incubating in piranha [3:1 H_2SO_4 (concentrated):H_2O_2 (30%), v/v] followed by rinsing with nanopure water and drying under a stream of N_2. After the nanocrystal ink was completely dried on the PDMS, the stamp was placed in a custom built stamping jig and pressure molded onto the substrate.

Diffraction Efficiency (DE) Measurements. Measurements were taken at normal incidents with the radiation impingent on the glass side of the ITO-coated glass substrate. The grating was placed at the center of a rotation stage, while a wavelength-sensitive photodetector (Newport 1930c) was rotated around the sample in order to take power measurements at the $m = 1$, 0, and −1 spots. An argon ion (488 nm, *ca.* 1.5 mW) and a HeNe (633 nm, *ca.* 150 μW) laser were used. All reported values for DE are the average of three different samples, in which three different areas were interrogated per sample (*i.e.*, the values are an average of a total of 9 values). When necessary to maintain consistency when comparing samples, optical density (OD) of the samples was calculated as the log of the ratio of the sum of the transmitted spots (I_{trans}; $m = 1$, 0, and −1) to the incident laser power (I_o) [OD = log ($I0_o/I_{trans}$)].

Nanocrystal and Grating Characterization. FE-SEM images of nanocrystal gratings were taken on a Hitachi S-4800 at an accelerat-

ing voltage of 15 kV and a tip current of 10 μA. Optical absorption spectra were taken on an Agilent 8453A linear diode array spectrophotometer. TGA data was acquired for samples of greater than 2 mg on a TA Instruments 2900 series instrument at a rate of 10 °C/minute, from 50 to 600 °C. AFM measurements were performed on a Digital Instruments Dimension 3100 Scanning Probe Microscope in tapping mode.

Acknowledgment. Full or partial support of this research was provided by the National Science Foundation (CHE 0517963), the NSF Science and Technology Center for Materials and Devices for Information Technology Research (DMR DMR-0120967), and the Department of Energy Basic Energy Sciences (DE-FG03-02ER15753).

Supporting Information Available: SEM images for determining QD grating feature sizes in Table 1; comprehensive DE data for each CdSe NC size/concentration solution; UV−visible spectra for each CdSe NC diameter; and TGA for each purified QD sample diameter. This material is available free of charge *via* the Internet at http://pubs.acs.org.

REFERENCES AND NOTES

1. Bowles, S. E.; Wu, W.; Kowalewski, T.; Schalnat, M. C.; Davis, R. J.; Pemberton, J. E.; Shim, I.; Korth, B. D.; Pyun, J. Magnetic Assembly and Pyrolysis of Functional Ferromagnetic Colloids into One-Dimensional Carbon Nanostructures. *J. Am. Chem. Soc.* **2007**, *129*, 8694–8695.
2. Keng, P. Y.; Shim, I.; Korth, B. D.; Douglas, J. F.; Pyun, J. Synthesis and Self-Assembly of Polymer-Coated Ferromagnetic Nanoparticles. *ACS Nano* **2007**, *1*, 279–292.
3. Korth, B. D.; Keng, P.; Shim, I.; Bowles, S. E.; Tang, C.; Kowalewski, T.; Nebesny, K. W.; Pyun, J. Polymer-Coated Ferromagnetic Colloids from Well-Defined Macromolecular Surfactants and Assembly into Nanoparticle Chains. *J. Am. Chem. Soc.* **2006**, *128*, 6562–6563.
4. Kim, L.; Anikeeva, P. O.; Coe-Sullivan, S. A.; Steckel, J. S.; Bawendi, M. G.; Bulovic, V. Contact Printing of Quantum Dot Light-Emitting Devices. *Nano Lett.* **2008**, *8*, 4513–4517.
5. Wu, X. C.; Lenhert, S.; Chi, L. F.; Fuchs, H. Interface Interaction Controlled Transport of CdTe Nanoparticles in the Microcontact Printing Process. *Langmuir* **2006**, *22*, 7807–7811.
6. Wu, X. C.; Bittner, A. M.; Kern, K. Microcontact Printing of CdS/Dendrimer Nanocomposite Patterns on Silicon Wafers. *Adv. Mater.* **2004**, *16*, 413–417.
7. Pattani, V. P.; Li, C. F.; Desai, T. A.; Vu, T. Q. Microcontact Printing of Quantum Dot Bioconjugate Arrays for Localized Capture and Detection of Biomolecules. *Biomed. Microdevices* **2008**, *10*, 367–374.
8. Chen, J.; Liao, W.-S.; Chen, X.; Yang, T.; Wark, S. E.; Son, D. H.; Batteas, J. D.; Cremer, P. S. Evaporation-Induced Assembly of Quantum Dots into Nanorings. *ACS Nano* **2009**, *3*, 173–180.
9. Cui, Y.; Bjork, M. T.; Liddle, J. A.; Sonnichsen, C.; Boussert, B.; Alivisatos, A. P. Integration of colloidal nanocrystals into lithographically patterned devices. *Nano Lett.* **2004**, *4*, 1093–1098.
10. Tao, A. R.; Huang, J. X.; Yang, P. D. Langmuir−Blodgettry of Nanocrystals and Nanowires. *Acc. Chem. Res.* **2008**, *41*, 1662–1673.
11. Lu, Y.; Liu, G. L.; Lee, L. P. High-Density Silver Nanoparticle Film with Temperature-Controllable Interparticle Spacing for a Tunable Surface Enhanced Raman Scattering Substrate. *Nano Lett.* **2005**, *5*, 5–9.
12. Gattas-Asfura, K. M.; Constantine, C. A.; Lynn, M. J.; Thimann, D. A.; Ji, X. J.; Leblanc, R. M. Characterization and 2D Self-Assembly of CdSe Quantum Dots at the Air−Water Interface. *J. Am. Chem. Soc.* **2005**, *127*, 14640–14646.
13. Chan, Y. T.; Snee, P. T.; Caruge, J. M.; Yen, B. K.; Nair, G. P.; Nocera, D. G.; Bawendi, M. G. A Solvent-Stable Nanocrystal-Silica Composite Laser. *J. Am. Chem. Soc.* **2006**, *128*, 3146–3147.
14. Snee, P. T.; Chan, Y. H.; Nocera, D. G.; Bawendi, M. G. Whispering-Gallery-Mode Lasing from a Semiconductor Nanocrystal/Microsphere Resonator Composite. *Adv. Mater.* **2005**, *17*, 1131–1136.
15. Chan, Y.; Steckel, J. S.; Snee, P. T.; Caruge, J. M.; Hodgkiss, J. M.; Nocera, D. G.; Bawendi, M. G. Blue Semiconductor Nanocrystal Laser. *Appl. Phys. Lett.* **2005**, *86*, 4614–4616.
16. Chan, Y.; Caruge, J. M.; Snee, P. T.; Bawendi, M. G. Multiexcitonic Two-State Lasing in a CdSe Nanocrystal Laser. *Appl. Phys. Lett.* **2004**, *85*, 2460–2462.
17. Tian, S. J.; Armstrong, N. R.; Knoll, W. Electrochemically Tunable Surface-Plasmon-Enhanced Diffraction Gratings and Their (Bio-)sensing Applications. *Langmuir* **2005**, *21*, 4656–4660.
18. Marikkar, F. S.; Carter, C.; Kieltyka, K.; Robertson, J. W. F.; Williamson, C.; Simmonds, A.; Zangmeister, R.; Fritz, T.; Armstrong, N. R. Conducting Polymer Diffraction Gratings on Gold Surfaces Created by Microcontact Printing and Electropolymerization at Submicron Length Scales. *Langmuir* **2007**, *23*, 10395–10402.
19. Schanze, K. S.; Bergstedt, T. S.; Hauser, B. T.; Cavalaheiro, C. S. P. Photolithographically-Patterned Electroactive Films and Electrochemically Modulated Diffraction Gratings. *Langmuir* **2000**, *16*, 795–810.
20. Schanze, K. S.; Bergstedt, T. S.; Hauser, B. T. Photolithographic Patterning of Electroactive Polymer Films and Electrochemically Modulated Optical Diffraction Gratings. *Adv. Mater.* **1996**, *8*, 531.
21. Massari, A. M.; Stevenson, K. J.; Hupp, J. T. Development and Application of Patterned Conducting Polymer Thin Films As Chemoresponsive and Electrochemically Responsive Optical Diffraction Gratings. *J. Electroanal. Chem.* **2001**, *500*, 185–191.
22. Fayer, M. D. Dynamics of Molecules in Condensed Phases—Picosecond Holographic Grating Experiments. *Annu. Rev. Phys. Chem.* **1982**, *33*, 63–87.
23. Peng, X. G.; Thessing, J. Controlled Synthesis of High Quality Semiconductor Nanocrystals. In *Semiconductor Nanocrystals and Silicate Nanoparticles*; Structure and Bonding Series, Vol. 118; Springer: Berlin, 2005; pp 79−119.
24. Wang, L. W.; Zunger, A. Pseudopotential Calculations of Nanoscale CdSe Quantum Dots. *Phys. Rev. B* **1996**, *53*, 9579–9582.
25. Yu, W. W.; Qu, L. H.; Guo, W. Z.; Peng, X. G. Experimental Determination of the Extinction Coefficient of CdTe, CdSe, and CdS Nanocrystals. *Chem. Mater.* **2003**, *15*, 2854–2860.
26. Xia, Y. N.; Whitesides, G. M. Soft Lithography. *Angew. Chem., Int. Ed.* **1998**, *37*, 551–575.
27. Qu, L. H.; Peng, X. G. Control of Photoluminescence Properties of CdSe Nanocrystals in Growth. *J. Am. Chem. Soc.* **2002**, *124*, 2049–2055.
28. Brumbach, M.; Veneman, P. A.; Marrikar, F. S.; Schulmeyer, T.; Simmonds, A.; Xia, W.; Lee, P.; Armstrong, N. R. Surface Composition and Electrical and Electrochemical Properties of Freshly Deposited and Acid-Etched Indium Tin Oxide Electrodes. *Langmuir* **2007**, *23*, 11089–11099.
29. Foos, E. E.; Wilkinson, J.; Makinen, A. J.; Watkins, N. J.; Kafafi, Z. H.; Long, J. P. Synthesis and Surface Composition Study of CdSe Nanoclusters Prepared Using Solvent Systems Containing Primary, Secondary, and Tertiary Amines. *Chem. Mater.* **2006**, *18*, 2886–2894.
30. Luther, J. M.; Law, M.; Song, Q.; Perkins, C. L.; Beard, M. C.; Nozik, A. J. Structural, Optical and Electrical Properties of Self-Assembled Films of PbSe Nanocrystals Treated with 1,2-Ethanedithiol. *ACS Nano* **2008**, *2*, 271–280.
31. Plowman, T. E.; Saavedra, S. S.; Reichert, W. M. Planar Integrated Optical Methods for Examining Thin Films and Their Surface Adlayers. *Biomaterials* **1998**, *19*, 341–355.
32. Yang, L.; Saavedra, S. S.; Armstrong, N. R.; Hayes, J. Fabrication and Characterization of Low-Loss, Sol−Gel Planar Wave-Guides. *Anal. Chem.* **1994**, *66*, 1254–1263.